

# CORRECTION OF SYSTEMATIC RADIOMETRIC INHOMOGENEITY IN SCANNED AERIAL CAMPAIGNS USING PRINCIPAL COMPONENT ANALYSIS

XXXXXX XXXXX \*

XXXXXX XXXX XXXXXXXX XXXXXXXXXXXX XXXXXXXX XXXXX XXXX  
(XXXXXX.XXXX)@XXXX.XXX

Commission III (?)

**KEY WORDS:** Analogue Photography, Airborne Imagery, Radiometry, Orthophotomosaic, Hotspot Correction, PCA, KLT

## ABSTRACT:

Orthophotomosaic is defined as a single image that can be layered on a map. The term “mosaic” implies that it is produced from a set of images, usually aerial images. Even if these images are taken during cloudless period, they are impaired by radiometric inhomogeneity mostly due to atmospheric phenomena, like hotspot, haze or high altitude clouds shadows as well as imaging device systematisms, like lens vignetting. These create some unsightly radiometric inhomogeneity in the orthophotomosaic that could be corrected by using a Wallis filter. Yet this solution leads to a significant loss of contrast at small scales. This work introduces an alternative to Wallis filter by considering some systematic radiometric behaviours in the images through a principal component analysis process.

## 1. INTRODUCTION

### 1.1 Context of our work

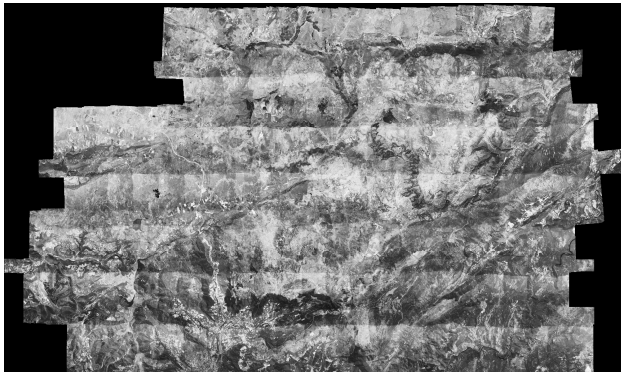


Figure 1(a). Orthophotomosaic with overlaps

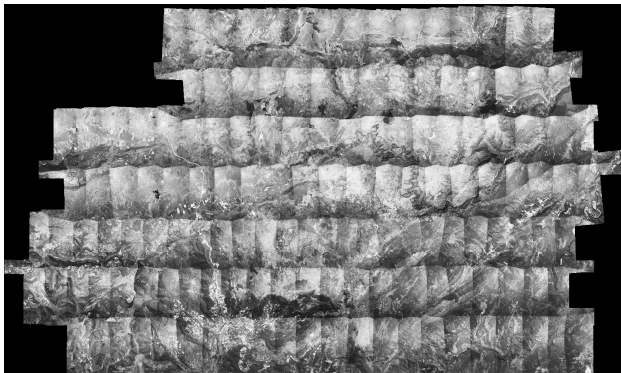


Figure 1(b). Orthophotomosaic with Voronoi cells

Working on former aerial campaigns has become a major issue in remote sensing and, more generally, in data sciences with European projects like Time Machine or more local project like Swisstopo historical scanned maps or French National Mapping Agency scanned aerial campaigns available on the website IGN Remonter le Temps.

These data are interesting for at least two reasons. First, they don't need specific acquisition, just scanning the archives, which is a cost-effective way to obtain data. Second, they open new research opportunity, for example in the studies of time varying phenomena. Yet, their exploitation leads to some issues. In this work, we will specifically take an interest in the radiometric issues in scanned analogue airborne images.

### 1.2 Dataset

Our dataset is only composed of images. Unlike recent aerial campaigns, don't have information about the exposure time nor the camera calibration, yet we assume that they were shot with the same camera and following the same acquisition pattern (Abdullah et al., 2013) which consists on several stripes, with overlaps to ensure stereographic interpretation. These images are also orthorectified using the software MicMac (Rupnik et al., 2017). A product of this orthorectification is an orthophotomosaic shown on Figure 1(a,b).

There are two ways of mosaicking per image orthophoto: using the overlaps like in Figure 1(a) where each pixel is the mean of the different contributing images or choosing the contribution of only one image per pixel, usually the one which the centre is the closest to the considered pixel like in Figure 1(b).

Both rendering methods have their pros and cons: the radiometry of Figure 1(a) seems more homogeneous yet small shift between the different images could be observed at full

\* Corresponding author

resolution whereas the inhomogeneity of Figure 1(b) is more pronounced. In any case, both rendering are presenting radiometric inhomogeneity requiring a correction step.

### 1.3 Existing approaches

**1.3.1 Statistic approaches:** The image correction currently used, for example on the historical images from IGN Remont le Temps, is purely image based and lays on Wallis filtering (Wallis, 1976) illustrated by Figures 2, 3 and 4. When considering Figure 2, one notices that the contrast perception is not the same at each scales: small scales suffer from a loss of contrast whereas large scales (full resolution zoom) do not present any visible contrast alteration.

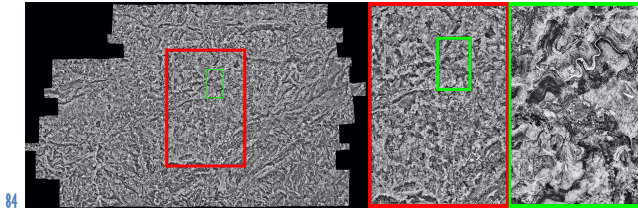


Figure 2. Wallis filter solution viewed at different scale

Some more recent works using Contourlet transform (Li, 2016) are also returning unsatisfying results when considered at small scales.

**1.3.2 Multi-scales approaches:** In order to perform correction at different scales, one could consider multi-resolution blending (Ogden, 1985) mostly used in panoramic image rendering (Brown et al., 2007) yet requiring a preliminary vignetting (image radial darkening) correction. The main issue in our case is that we don't know the vignetting parameters.

**1.3.3 Physical approaches:** Vignetting is mostly due to two factors: the constant lens vignetting and the hotspot which could be determined by the Sun position. Knowing these parameters and using a physical model (Chandelier, 2009). Unfortunately, the Sun position, given by the date and the time of the aerial shot should be determined for each image, in addition of other parameters (like the aerosol composition of the atmosphere or the film response curve) that cannot be obtained on old scanned airborne missions. Consequently, physically bases radiometric correction cannot be performed in our case.

## 2. PROPOSED APPROACH

Our approach is purely image based and could be come down to a Wallis filtering method regularized by all the images of a mission, the parameters of the filter being obtained by principal component analysis (PCA), also known under the name of Karhunen-Loève transform (KLT).

### 2.1 Wallis filtering

The principle is illustrated by the Figure 3. There are only three parameters: the size of the window, the desired mean (for example 128, in the case of an 8bit image) and the desired standard deviation (for example a value between 32 or 64). The mean and the standard deviation would be respectively influencing the luminosity and the contrast of the resulting image.

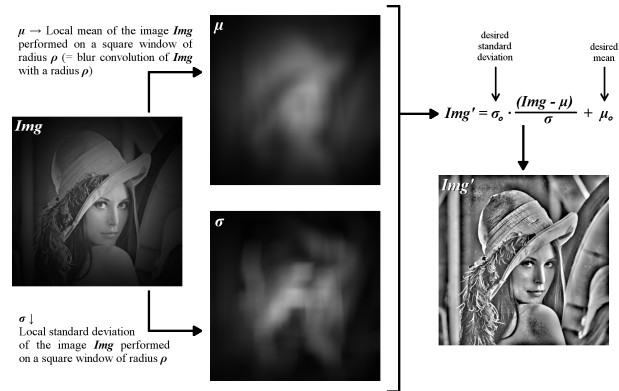


Figure 3. Wallis filtering

The influence of the window is shown in Figure 4. A small window will remove the vignetting and all the low frequencies of the image whereas a large window will keep the image vignetting uncorrected. The size of the window is chosen empirically to obtain an acceptable compromise between vignetting correction and image legibility.



Figure 4. Influence of the size ( $w$ ) of the window

Yet, even after choosing manually an optimal window, the final orthophotomosaic rendering is not satisfying at small scales as shown previously on Figure 2.

In other words, this method is equivalent to calculate a gain and an offset for each pixel according to it neighbourhood.

### 2.2 Karhunen-Loève transform

This method, based on principal component analysis, is illustrated by Figure 5. A set of vector of the same length, in our case images represented on a canonical basis are processed to generate a new basis, called KLT basis, where most of the information is given by the first vectors, the other vectors would give more specific information. In another way, the first vectors will show the systematic behaviours of the vector set. In the case of images, they correspond to common global behaviours shared by all the images.

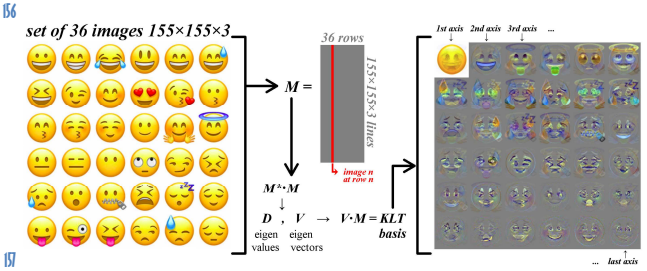


Figure 5. Karhunen-Loève transform (KLT)

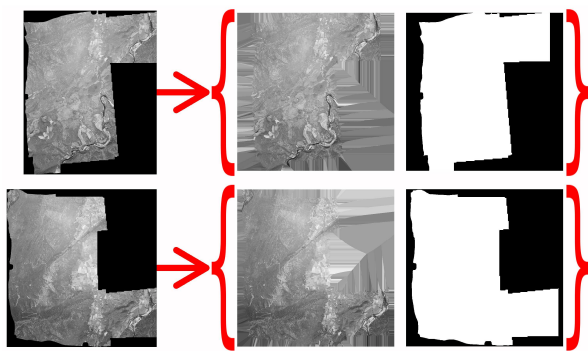
In our case the input vectors would be of two kind: the locals mean of each aerial images and their local standard deviation (for a given Wallis filtering window). For each image a new

163 local mean and a new local standard deviation is determined  
 164 using only the first vectors of the KLT basis. Using all the  
 165 vectors from the KLT basis to reconstruct the local means and  
 166 standard deviation would lead to the initial Wallis filtering  
 167 shown in Figure 2.

168  
 169 Principal component analysis acts here to some extent as a low  
 170 pass filter: The first axes of the KLT basis are displaying some  
 171 low frequencies or small scales behaviour of the dataset.

### 172 2.3 Preparing the images

174 To obtain a KLT basis, the vector, derived from the aerial  
 175 orthorectified images, should have the same size, which is not  
 176 the case. In order to give all the images the same size without  
 177 losing information, instead of cropping them, it was decided to  
 178 include them in a bigger square frame completed by nearest  
 179 neighbourhood extrapolation. Each new resized image has a  
 180 mask and a new orientation file (because we are working with  
 181 orthorectified images). Some examples are given in Figure 6.



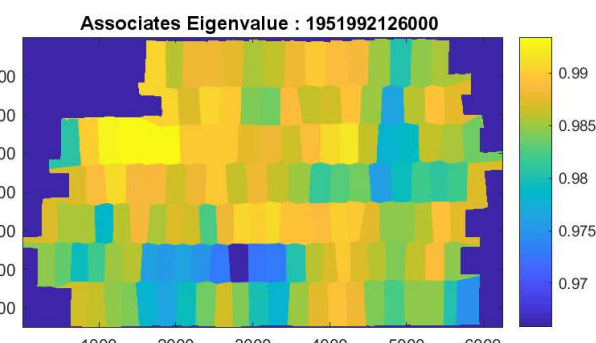
183  
 184 Figure 6. Two extrapolated images with their associated mask

185  
 186 The extrapolation is justified by the fact that using directly the  
 187 images with their mask would follow some irrelevant KLT basis  
 188 illustrated in Appendix A.

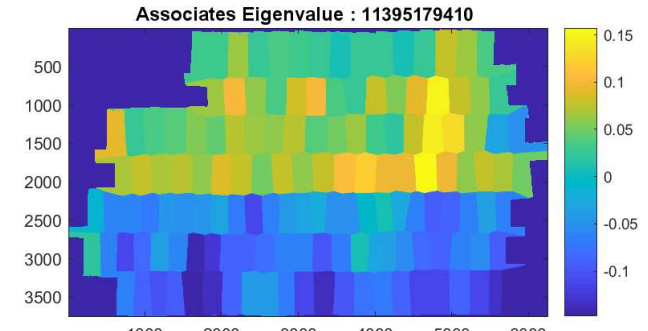
189  
 190 As the phenomena that have to be corrected are related to very  
 191 low frequencies, in other word very small scales, working on  
 192 low resolution images is justified. Images size is 800x800 pixels

## 193 3. RESULTS

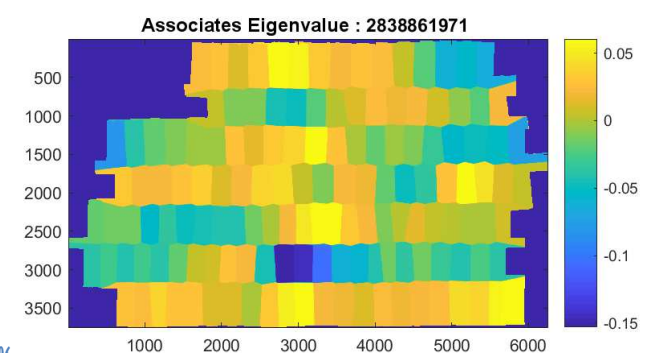
195 The data set is composed of 143 orthorectified images shot with  
 196 an analogue camera in the Larzac (France) in 1996. Computing  
 197 the KLT basis of this set leads to 143 “eigen” images (KLT  
 198 axis) associated to respective eigenvalues. Only the ones with  
 199 stronger eigenvalues will be considered.



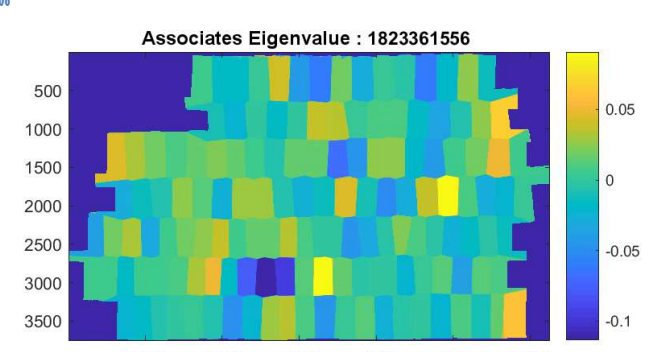
200  
 201 Figure 7(a). Correlation with the first KLT axis (local mean)



202  
 203 Figure 7(b). Correlation with the second KLT axis (local mean)



204  
 205 Figure 7(c). Correlation with the third KLT axis (local mean)



206  
 207 Figure 7(d). Correlation with the fourth KLT axis (local mean)

### 208 3.1 Choosing the relevant number of KLT axis

209  
 210 The choice of the “threshold” will be empirical (yet, justified by  
 211 some observations). Let’s consider the correlation of each  
 212 image with the vector axis of the KLT basis which main axes are  
 213 shown at Figure 8.

214  
 215 The results are shown in Figures 7(a,b,c,d). All the images are  
 216 strongly correlated with the first axis: this is the main behaviour  
 217 of our images set. The second axis is more interesting: two  
 218 distinct behaviours are observed on Figure 7(b) between the  
 219 North and the South of the mission. After considering the  
 220 “eigen” image relative to the second axis, this could be  
 221 interpreted as a change of the hotspot shape, probably due to a  
 222 different position of the Sun. Further investigation showed that  
 223 the images were not taken the same day; it was a two days  
 224 mission. The correlation with the third or fourth (Figures 7(c,d))  
 225 axis is more difficult to interpret: the variation seems somehow

more or less correlated along one strip. The correlations on other axis do no show structured behaviour.

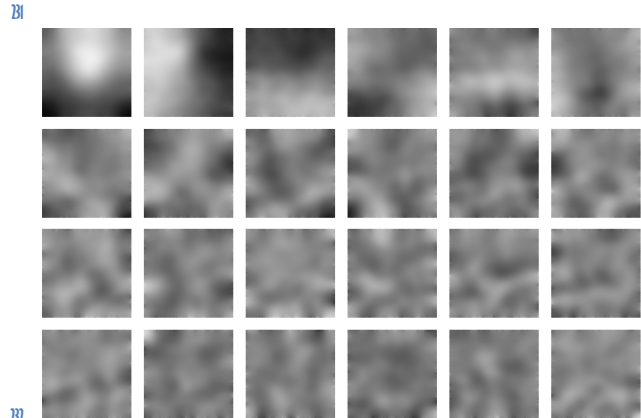


Figure 8. The 24 main KLT axis (local mean) sorted by their decreasing eigenvalues

So only the three (or four) first axis seem relevant to model the local means and standard deviations of each image, the other orders axis being not correlated with systematic phenomena that we try to remove.

### 3.2 Orthophotomosaic rendering

In order to compare and discuss our results in a more visual and efficient way, the Figures 9(a,b,c,d) are represented in colour scale instead of greyscale.

Compared to uncorrected overlap rendered orthophotomosaic (Figure 9(a)), our results are more homogeneous even if some little discontinuities seem to be present in the Voronoi cell reconstruction (Figure 9(c)). These discontinuities are almost invisible in the overlap reconstruction (Figure 9(d)).

A compromise is obtained by merging the two reconstructions: in practice, applying another Wallis filter on the corrected images where the desired mean and standard deviation are no more fixed but given by the overlaps rendered orthophotomosaic: the details coming from the Voronoi cells rendering and the low frequencies from the overlaps rendering.

Eventually, our method avoids the loss of contrast following the Wallis filtering approach (Figure 9(b)). Yet, some initial choices could be discussed and developed.

### 3.3 Discussion and further developments

This method is justified by the fact that our set is composed of a large amount of images yet on small sets of images, this method would probably show some limits. The fact we are using orthorectified images instead of considering directly the images in the camera geometry might be justified by the assumption that oriented images would give better results, yet restarting the experiment directly on the “raw” images could be an interesting alternative approach to this method.

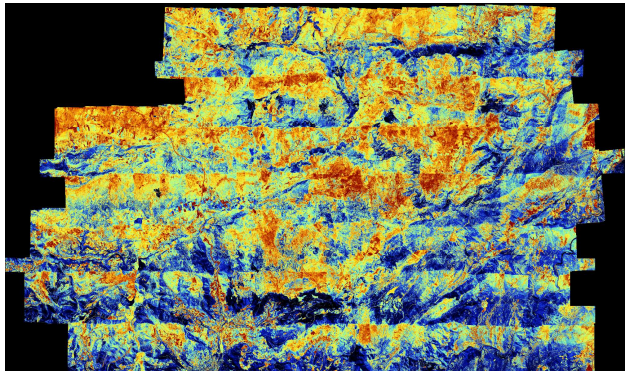


Figure 9(a).Orthophotomosaic with uncorrected overlaps

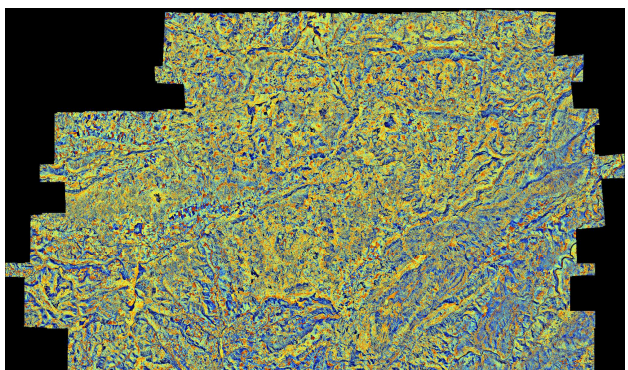


Figure 9(b).Orthophotomosaic corrected with simple Wallis

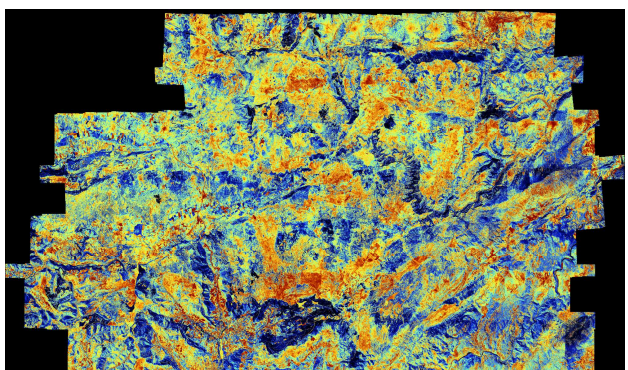


Figure 9(c).Our result rendered with Voronoi cells

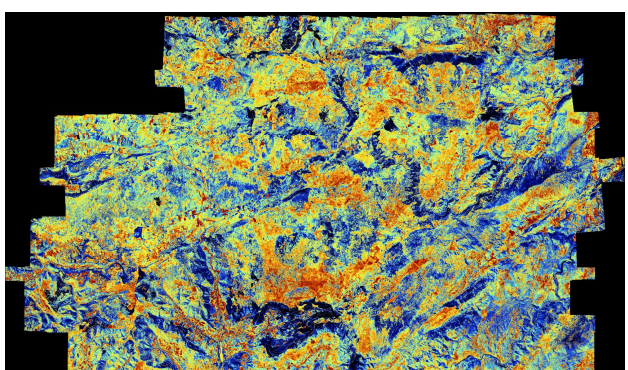


Figure 9(d). Our result rendered with overlaps

#### 4. PERSPECTIVES

186 Compared to existing methods of radiometric correction,  
 187 without any context information, our simple approach gives  
 188 better visual results. Yet, this method is only limited to  
 189 panchromatic images. Applying it directly on colour images  
 190 (separately on red, green and blue bands) leads to some  
 191 unsightly results shown in Appendix B. The colour approach  
 192 should be considered in a different way, typically by first  
 193 avoiding using fixed global mean and standard deviation as it is  
 194 done in this work.

195

196 Another perspective would be to perform our method directly  
 197 on “raw” images and see its influence on the photogrammetric  
 198 process leading to final product as digital terrain model and  
 199 orthorectified images. Eventually, the last step would consist on  
 200 testing our method on larger datasets, like for example a region  
 201 or a whole country in order to discuss its possible limits.

202

#### REFERENCES

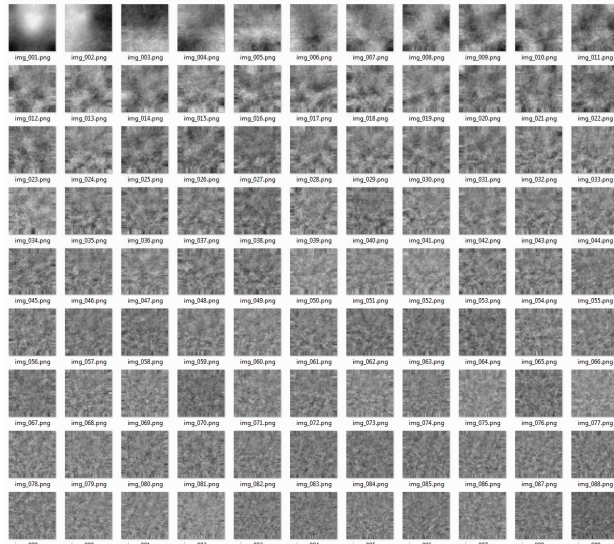
- 304 Abdullah, Q., Bethel, J., Hussain, M. & Munjy, R.  
 305 Photogrammetric project and mission planning. In: McGlone,  
 306 J.C. (Ed.), *Manual of Photogrammetry*. American Society for  
 307 Photogrammetry and Remote Sensing 1187–1220 (2013).
- 308
- 309 Brown, M. & Lowe, D.G. Automatic Panoramic Image  
 310 Stitching using Invariant Features. *Int J Comput Vision* 74, 59–  
 311 73 (2007). <https://doi.org/10.1007/s11263-006-0002-3>
- 312
- 313 Chandelier, L. & Martinoty, G. A Radiometric Aerial  
 314 Triangulation for the Equalization of Digital Aerial Images and  
 315 Orthoimages, *Photogrammetric Engineering & Remote*  
 316 *Sensing*, Number 2 / February 2009, pp. 193-200(8).  
 317 <https://doi.org/10.14358/PERS.75.2.193>
- 318
- 319
- 320 IGN Remonter le Temps, <https://remonterletemps.ign.fr> (link  
 321 visited on February the 6th, 2020)
- 322
- 323 Li, W., Sun, K., Li, D., & Bai, T. Algorithm for automatic  
 324 image dodging of unmanned aerial vehicle images using two-  
 325 dimensional radiometric spatial attributes, *Journal of Applied*  
 326 *Remote Sensing* 10(3), 036023 (12 September 2016).  
 327 <https://doi.org/10.1111/1.JRS.10.036023>
- 328
- 329 MicMac, <https://micmac.ensg.eu> (link visited on February the  
 330 6th, 2020)
- 331
- 332 Ogden, M., Adelson, E.H., Bergen, J.R. & Burt, P.J. Pyramid-  
 333 based computer graphics. *RCA Engineer*, 30(5), 1985.
- 334
- 335 Rupnik, E., Daakir, M. & Pierrot Deseilligny, M. MicMac – a  
 336 free, open-source solution for photogrammetry. *Open*  
 337 *geospatial data, softw. stand.* 2, 14 (2017).  
 338 <https://doi.org/10.1186/s40965-017-0027-2>
- 339
- 340 SwissTopo, <https://www.swisstopo.admin.ch/en/maps-data-online/maps-geodata-online/journey-through-time.html> (link  
 341 visited on February the 6th, 2020)
- 342
- 343 Time Machine, *This project has received funding from the*  
 344 *European Union’s Horizon 2020 research and innovation*  
 345 *programme under grant agreement No 820323,*  
 346 <https://www.timemachine.eu> (link visited on February the 6th,  
 347 2020)
- 348
- 349 Wallis, R.H. An Approach to the Space Variant Restoration and  
 350 Enhancement of Images. *Proceedings of the Symposium on*  
 351 *Current Mathematical Problems in Image Science*, Monterey,  
 352 10-12 November 1976
- 353

35

## APPENDIX A

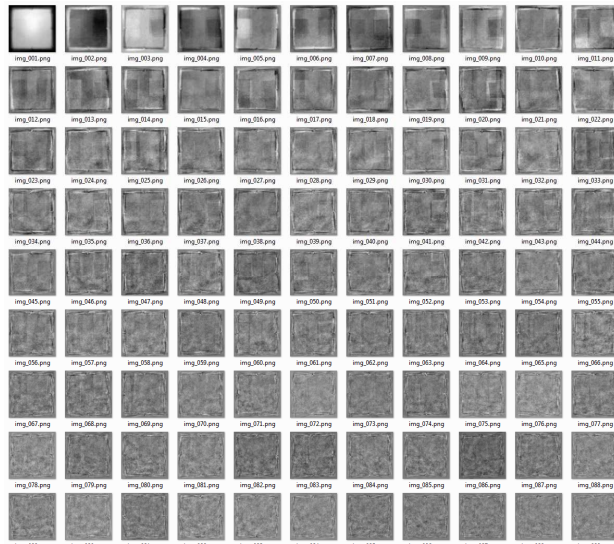
36 The 99 first axis of the KLT basis with and without  
37 extrapolation on the image border mask:

38



39

360



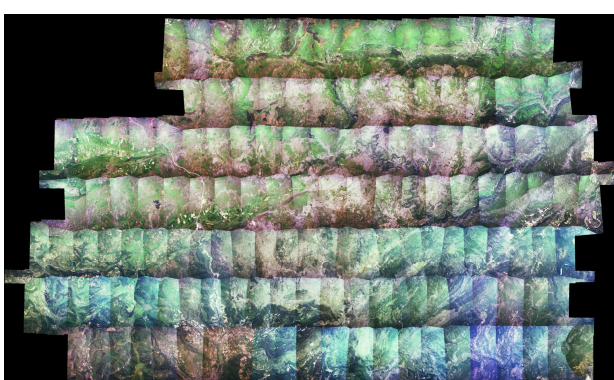
361

362

363

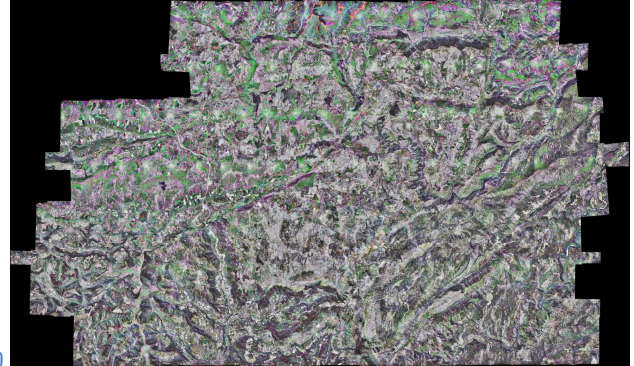
## APPENDIX B

364 From top to bottom: colour orthophotomosaic rendered without  
365 correction, with Wallis filtering on the RGB layer, with our  
366 method applied directly on the RGB layers:  
367



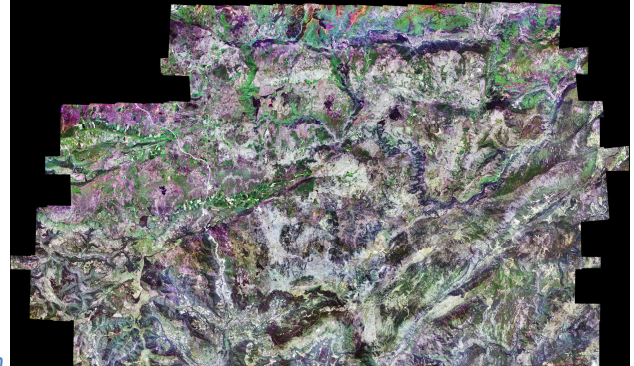
368

369



370

371



372

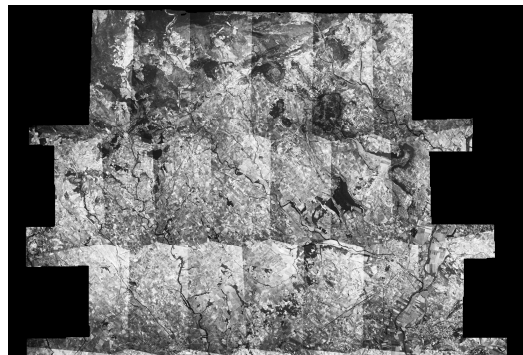
373

374

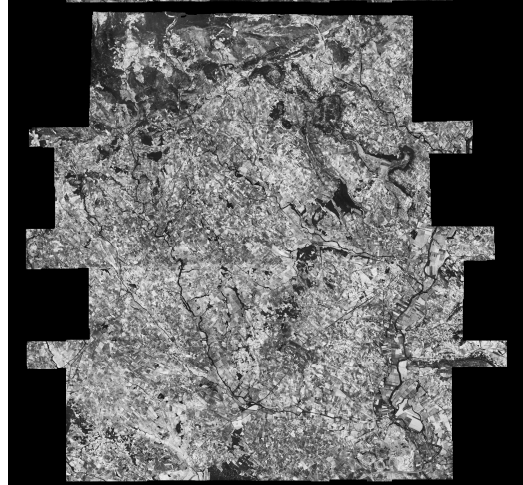
## APPENDIX C

375 More results on a smaller campaign with 27 images:

376



377



378

379